

Article

Remote Sensing for Water Quality Monitoring—A Case Study for the Marateca Reservoir, Portugal

Cristina Alegria ^{1,2}  and Teresa Albuquerque ^{1,2,3,*} 

¹ Instituto Politécnico de Castelo Branco, Polytechnic University of Castelo Branco, 6000-084 Castelo Branco, Portugal; crisalegria@ipcb.pt

² CERNAS-IPCB—Pólo de Castelo Branco do Centro de Estudos de Recursos Naturais, Ambiente e Sociedade, Unidade de Investigação e Desenvolvimento do Instituto Politécnico de Castelo Branco, 6000-084 Castelo Branco, Portugal

³ Institute of Earth Sciences (IES), University of Évora Pole, 7004-516 Evora, Portugal

* Correspondence: teresal@ipcb.pt

Abstract: Continuous monitoring of water resources is essential for ensuring sustainable urban water supply. Remote sensing techniques have proven to be valuable in monitoring certain qualitative parameters of water with optical characteristics. This survey was conducted in the Marateca reservoir located in central inland Portugal, after a major event that killed a considerable number of fish. The objectives of the study were as follows: (1) to define a pollution spectral signature specific to the Marateca reservoir that could shed light on the event; (2) to validate the spectral water's quality characteristics using the data collected in five gauging points; and (3) to model the characteristics of the reservoir water, including its depth, trophic state, and turbidity. The parameters considered for analysis were total phosphorus, total nitrogen, and chlorophyll-a, which were used to calculate a trophic level index. Sentinel-2 imagery was employed to calculate spectral indices and image ratios for specific bands, aiming at the definition of spectral signatures, and to model the water characteristics in the reservoir. The trophic level index acquired from each of the five gauging points was used for validation purposes. The reservoir's trophic level was classified as hypereutrophic and eutrophic, indicating its sensitivity to contamination. The developed methodological approach can be easily applied to other reservoirs and serves as a crucial decision-making tool for policymakers.

Keywords: trophic level index; spectral indices change; spectral signatures; random forest algorithm



Citation: Alegria, C.; Albuquerque, T. Remote Sensing for Water Quality Monitoring—A Case Study for the Marateca Reservoir, Portugal. *Geosciences* **2023**, *13*, 259. <https://doi.org/10.3390/geosciences13090259>

Academic Editor: Tobias Nilsson

Received: 26 July 2023

Revised: 20 August 2023

Accepted: 21 August 2023

Published: 24 August 2023



Copyright: © 2023 by the authors. Licensee MDPI, Basel, Switzerland. This article is an open access article distributed under the terms and conditions of the Creative Commons Attribution (CC BY) license (<https://creativecommons.org/licenses/by/4.0/>).

1. Introduction

The need for sustainable urban water supplies necessitates continuous monitoring of the quality of available water resources and their watersheds. Trophic classifications are important tools for aquatic research, as they allow for a deeper understanding of surface water's ecosystems functioning. Aquatic pollution is a pressing environmental concern that has garnered significant attention in scientific research and in the literature [1–7]. The delicate balance of our water ecosystems is under threat due to various human activities, leading to the emergence of numerous pollutants that endanger aquatic life and ecosystem health. In this context, some indicators of aquatic pollution have become prominent subjects of study and discourse in the scientific community [3,6,7]. Thus, it is essential to continually monitor and assess these indicators to gauge the extent of aquatic pollution and implement effective remediation strategies.

Common qualitative parameters of water measured using remote sensing include chlorophyll-a (Chl-a), colored dissolved organic matters (CDOMs), Secchi disk depth (SDD), turbidity, total suspended sediments (TSS), water temperature (WT), total phosphorus (TP), sea surface salinity (SSS), dissolved oxygen (DO), biochemical oxygen demand (BOD), and chemical oxygen demand (COD). Many of these parameters are correlated with each other [8–12].

The use of spectral information for automated pollution recognition is increasing in the literature [13–15]. In recent years, advances in remote sensing technology and data analysis have paved the way for innovative approaches to identify and track pollution sources. One such promising technique is the utilization of spectral information for automated pollution recognition. Spectral information refers to the measurement of electromagnetic radiation across various wavelengths. Different materials and substances have unique spectral signatures, which can be detected and analyzed using specialized sensors, such as spectrometers and hyperspectral imagers. These devices capture data in multiple narrow and contiguous bands, providing a comprehensive view of the reflected or emitted light from a target area [13–15]. The benefits of using spectral information for automated pollution recognition are numerous. First and foremost, it enables real-time or near-real-time monitoring, allowing for timely interventions to prevent further environmental degradation. Additionally, this approach covers vast geographic areas, providing a comprehensive understanding of pollution patterns and their sources. However, challenges do exist. Proper calibration, atmospheric correction, and data interpretation are essential to ensure the accuracy and reliability of spectral information [13–15]. Additionally, integrating spectral data into existing pollution monitoring systems and decision-making processes requires collaboration between environmental scientists, engineers, and policymakers. The use of spectral information for automated pollution recognition represents a significant step forward in environmental monitoring and management. By leveraging the power of remote sensing and spectral analysis, it is possible to enhance the ability to detect pollution sources promptly, take informed actions, and work towards a cleaner and healthier planet [16].

Efficient models have already been developed for chlorophyll-a (Ch-a), turbidity, dissolved oxygen (DO), and total phosphorus (TP) using single spectral bands, water spectral indices, and ratios derived from remote sensing imagery [9]. For instance, the Sentinel-2 Multispectral Imager (MSI) imagery and the corresponding Sentinel-3 Ocean and Land Color Instrument (OLCI) products have been employed in aquatic applications to assess chlorophyll-a (Chl-a) turbidity [10]. Spatial regression was used to map Chl-a using Sentinel-2 MSI imagery [11]. Other studies have used machine learning algorithms and several water spectral indices as explanatory variables to model a water quality index that combines nine non-correlated water quality parameters [12].

Climate change projections for Portugal indicate a notable rise in average air temperature, especially during the summer and in inland regions. However, precipitation forecasts remain uncertain, with most predictions suggesting a decrease in average rainfall and a shorter rainy season [17]. Official climate bulletins from IPMA (Portuguese Institute for the Sea and Atmosphere—IPMA) report a decline in precipitation since the early 21st century compared to the average precipitation between 1971 and 2000. The hydrological year of 2021/2022 was particularly dry, raising concerns about the water quality in reservoirs utilized for urban water supply.

The Marateca reservoir, situated in central inland Portugal, serves as the water source for the municipality of Castelo Branco and was chosen for a pilot survey to define pollution spectral signatures. A significant event occurred in April 2022, which spurred the purpose of this study—to define a pollution spectral signature specific to the Marateca reservoir that could shed light on the event. To ensure the validity of the findings, five gauging stations were used for validation purposes. Thus, the objectives of the study were as follows: (1) to define a pollution spectral signature specific to the Marateca reservoir that could shed light on the event; (2) to validate the spectral water's quality characteristics using the data collected in five gauging points; and (3) to model the characteristics of the reservoir water, including its depth, trophic state, and turbidity. The parameters considered for analysis were total phosphorus, total nitrogen, and chlorophyll-a, which were used to calculate a trophic level index. Sentinel-2 imagery was employed to calculate spectral indices and image ratios for specific bands, aiming at the definition of spectral signatures, and to model the water characteristics in the reservoir. The trophic level index acquired from each of the five gauging points was used for validation purposes.

2. Materials and Methods

2.1. Study Area

The Marateca reservoir is situated in the municipality of Castelo Branco, Portugal (Figure 1a,b). It is an embankment dam that was constructed in 1982 on the Ocreza River and became operational in 1991. The dam has a height of 25 m above its foundation (24 m above the natural terrain) and a crest length of 1054 m (with a width of 7.6 m). Its total storage capacity is 43.5 million m³. The dam has a bottom discharge capacity of 15.25 m³s^{−1} and a flood discharge capacity of 60 m³s^{−1}. At the full storage level, the reservoir covers an area of 6.34 km², and its total capacity is 37.2 million m³ (with a useful capacity of 32.7 million m³). The water levels in the reservoir are as follows: 385 m at full storage level (FSL), 385.5 m at maximum flood level, and 375.5 m at minimum exploration level [18]. According to the Portuguese Land Cover and Land Use (LCLU) thematic map of 2018 (COS2018) [19,20], the Marateca reservoir is predominantly surrounded by agricultural areas and grasslands (Figure 1c).

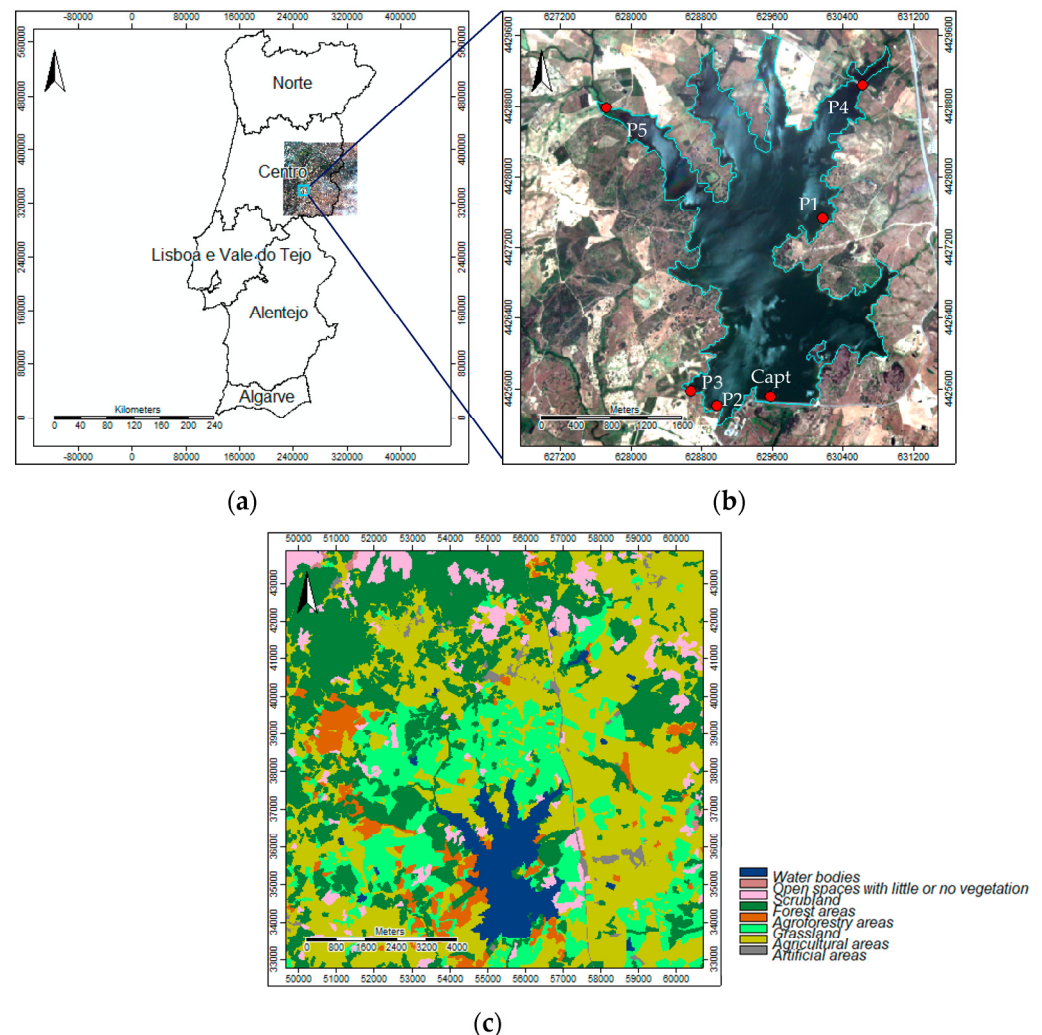


Figure 1. Study area: (a) Portugal and the Sentinel2A imagery tile (29 May 2022); (b) Marateca reservoir's limit from the LCLU (COS 2018), and the monitoring points (Capt, P1, P2, P3, P4, and P5); and (c) LCLU (COS 2018) around the Marateca reservoir.

2.2. Data

2.2.1. Climatological Data—Local Station

The climatological data were collected from the nearest local climate station to the study area in Castelo Branco, which is approximately 40 km away from the town. The

monthly climatological reports were downloaded from the official national portal of the Instituto Português do Mar e da Atmosfera (IPMA) [21].

For this study, climatological data from the hydrological years of 2021/2022 and 2022/2023 (spanning from October 2021 to January 2023) were used to analyze the monthly average temperatures (minimum and maximum, °C) and total monthly precipitation (in mm). These data were used to understand the observed changes in the study area during the aforementioned hydrological years (Figure 2).

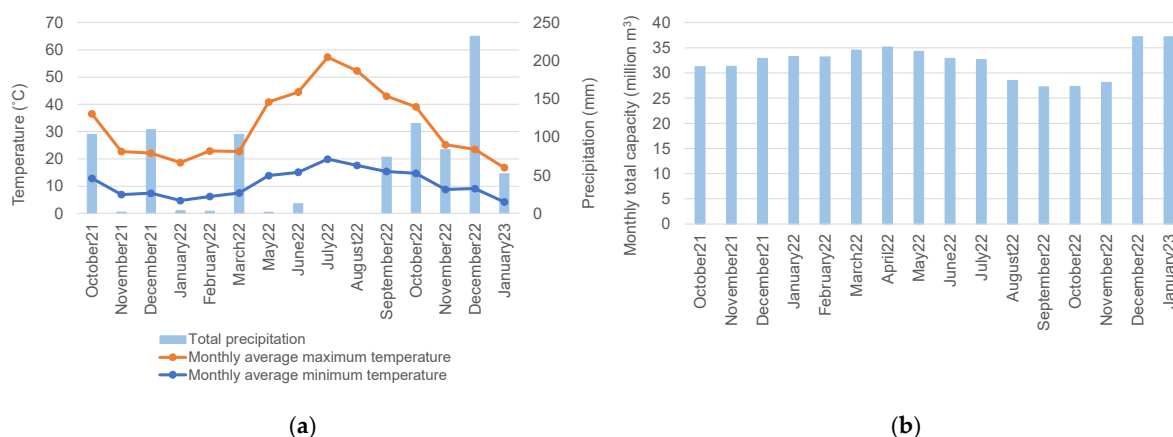


Figure 2. Study area: (a) Castelo Branco climatological station (October 2021–January 2023) data—monthly, average, minimum, and maximum temperatures and total monthly precipitation [21]; and (b) Marateca reservoir's monthly total capacity (million m³) (<https://snirh.apambiente.pt/index.php?idMain=2&idItem=3>, accessed on 22 March 2023).

2.2.2. Sentinel2A Imagery Data

The Sentinel-2A imagery data were obtained from the Copernicus program, the European Union's earth observation initiative. The data can be accessed through the program's website at <https://sentinels.copernicus.eu/web/sentinel/missions/sentinel-2>, accessed on 22 March 2023. Sentinel-2 is one of the missions under the Copernicus program. It currently operates two twin satellites, Sentinel-2A and Sentinel-2B, which provide high spatial resolution coverage (up to 10 m) and temporal resolution (every 5 days) [22]. The Sentinel-2 Multispectral Imager (MSI) imagery consists of 13 spectral bands, covering a range of 440 to 2180 nm, with spatial resolutions of 10, 20, and 60 m (Table 1).

Table 1. Sentinel-2 MSI—spectral bands and spatial resolution [23].

Band	Name	Central Wavelength (nm)	Spatial Resolution (m)
1	Coastal aerosol	443	60
2	Blue	490	10 and 20
3	Green	560	10 and 20
4	Red	665	10 and 20
5	Red-edge 1	705	20
6	Red-edge 2	740	20
7	Red-edge 3	783	20
8	NIR	842	10
8a	NIR narrow	865	20
9	Water vapour	945	60
10	Cirrus	1375	60
11	SWIR 1	1610	20
12	SWIR 2	2190	20

In this study, the Sentinel-2 Multispectral Instrument (MSI) imagery, Level 2A (atmospherically, radiometrically, and geometrically corrected), was downloaded for 16 monthly days of the last and current hydrological years (from October 2021 to January 2023) (Table 2).

Table 2. Sentinel-2A MSI imagery—dates of acquisition.

Year	Date of Acquisition											
	Jan	Feb	Mar	Apr	May	Jun	Jul	Aug	Sep	Oct	Nov	Dec
2021										11	30	30
2022	29	28	30	29	29	28	28	27	26		5 and 25	
2023	4 and 24											

2.2.3. Water Quality Parameters—Monitoring Points Data

The water quality parameters were obtained from the official national hydric resources information system, SNIRH (Sistema Nacional de Informação de Recursos Hídricos), which can be accessed through their website at <https://snirh.apambiente.pt/index.php?idMain=2&idItem=3>, accessed on 22 March 2023.

The Marateca reservoir is equipped with strategically placed monitoring points for measuring water quality (Figure 1b). The following parameters were considered: total phosphorus (TP), total nitrogen (TN), chlorophyll-a (Chl-a), total suspended solids (TSS), turbidity (TUR), and dissolved oxygen (DO).

The caption point (Capt) provided continuous data collection throughout the hydrological year of 2021–2022 for most of the parameters. On 27 April 2022 (Figure 3), data collection was conducted at almost all monitoring points (Capt, P1, P3, P4, and P5). However, the P2 point was not included for validation as there was no available information for 27 April 2022.

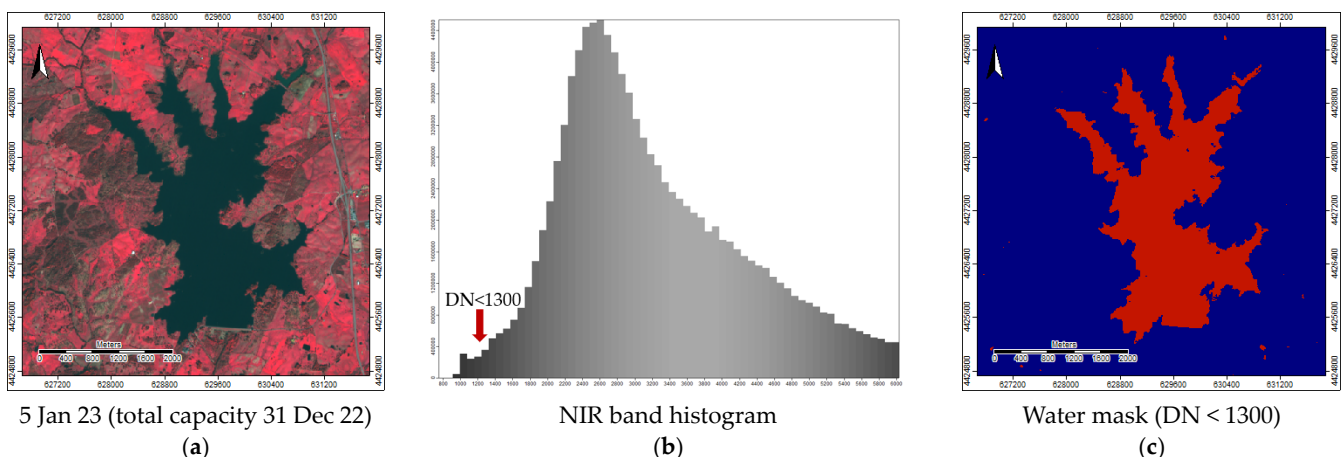


Figure 3. Study area—Marateca reservoir: (a) FCC at total capacity (e.g., 5 Jan 2023—37.2 million m³); (b) near-infrared band (NIR) histogram and threshold for the water mask; and (c) water mask (Boolean).

2.3. Methods

2.3.1. Composites, Spectral Indices, Ratios Imagery, and Spectral Signatures

A Geographical Information System (GIS) software called SAGA (System for Automated Geoscientific Analyses) was utilized for performing all computations with the Sentinel-2A imagery. SAGA is a free open-source software that can be accessed at <https://saga-gis.sourceforge.io/en/index.html>, accessed on 22 March 2023. The Coordinate System [EPSG 32629]: WGS84/UTM zone 29N was employed for the analysis.

For the 16 dates, false-color composites (FCCs) (Figure A1), spectral indices such as the normalized difference water index (NDWI) and normalized difference vegetation index (NDVI), as well as the spectral blue and green bands image ratio (B/G), were computed using imagery with a spatial resolution of 10 m (Table 3).

Table 3. Spectral indices and ratios (spatial resolution 10 m).

Acronym	Spectral Bands	Formula	Equation
NDWI	G—green band	$\frac{(G-NIR)}{(G+NIR)}$	$\frac{(B3-B8)}{(B3+B8)}$
	NIR—near infrared band		
NDVI	R—red band	$\frac{(NIR-R)}{(NIR+R)}$	$\frac{(B8-B4)}{(B8+B4)}$
	NIR—near infrared band		
B/G	B—blue band	$\frac{B}{G}$	$\frac{B2}{B3}$
	G—green band		

The NDWI values range from -1 to 1 , where water surfaces typically fall within the range of 0.2 to 1 . Flooding and high humidity are usually within the range of 0 to 0.2 , while moderate drought and non-aqueous surfaces are within -0.3 to 0 . Drought conditions and non-aqueous surfaces are within the range of -0.1 to -0.3 [24].

Regarding the NDVI values, they also range from -1 to 1 . Negative values correspond to water surfaces, manmade structures, rocks, clouds, and snow. Bare soil typically falls within the range of 0.1 to 0.2 , while plants always have positive values between 0.2 and 1 . A healthy, dense vegetation canopy should have an NDVI value above 0.5 , while sparse vegetation usually falls within the range of 0.2 to 0.5 [25].

In addition, monthly difference indices, namely dNDWI and dNDVI, were computed to highlight the changes observed in the Marateca reservoir from October 2021 to January 2023, particularly focusing on the periods between 30 March 2022 (pre-event), 29 April 2022 (post-event 1), and 29 May 2022 (post-event 2).

To delineate the Marateca reservoir, a single-band threshold approach was employed, based on the histogram of the Near-Infrared (NIR) band with a digital number (DN) threshold of less than 1300 . This threshold was determined using the NIR band histogram of the imagery taken at the total capacity day (e.g., 5 January 2023— 37.2 million m^3 ; Figure 2b). The result was a water mask in Boolean format (Figure 3), where water pixels are represented as “true” and non-water pixels as “false”. Subsequently, the water mask grid was converted into a shape format consisting of polygons. This shapefile was then utilized to extract the Marateca reservoir from the previously computed imagery with a spatial resolution of 10 m, including the NDWI, NDVI, B/G ratio, dNDWI, and dNDVI datasets.

The nine spectral bands (e.g., B, G, R, R-edge 1, R-edge 2, R-edge 3, NIR narrow, SWIR 1, and SWIR 2) with a spatial resolution of 20 m were utilized to acquire the spectral signatures at the monitoring points for the following dates: 30 March 2022 (pre-event), 29 April 2022 (post-event 1), and 29 May 2022 (post-event 2).

2.3.2. Water Quality Parameters—Monitoring and Validation Data

The 27 April 2022 was selected for validation purposes as a significant number of dead fish appeared all over the reservoir as reported by local news on the 10 April 2022.

The chosen parameters for water quality characterization were TP, TN, and estimated Chl- a^* values based on TP using the equation proposed by [26] (Equation (1)):

$$Ln(Chl-a) = \frac{(Ln(TP) + 2.5136)}{1.2354} \quad (1)$$

Trophic classifications for lakes are an important concern for aquatic scientists regarding the functioning of lake ecosystems [27–31]. In the realm of limnology and environmental science, the evaluation of water bodies’ health and nutrient enrichment is crucial. Trophic State Indices (TSIs) play a pivotal role in this assessment, offering a systematic approach to quantify the nutrient status and overall ecological condition of aquatic ecosystems. Over time, the TSI models have emerged in the literature, each designed to capture specific nuances and factors that influence trophic state dynamics. From the classic Carlson’s TSI [32], which relies on chlorophyll- a concentrations and transparency measurements, to more complex models the literature shows a range of different approaches. These models integrate various parameters such as nutrient concentrations (nitrogen and phosphorus),

water clarity, and even biological metrics like algal biomass and macrophyte coverage. General functional characteristics exist among the lakes in each of the main trophic status categories. Conceptually, it is common to consider three main groups: oligotrophic lakes, which have low nutrients, low algal biomass, high clarity, and deep photic zones; eutrophic lakes, where blooms of cyanobacteria are frequent, with high total nutrients; and mesotrophic lakes, which exhibit intermediate characteristics [30].

Additionally, a reservoir trophic level index (RTLI-(TP)), based on TP values, was calculated according to Lamparelli [26] (Equation (2)) as follows:

$$RTLI-(TP) = 10 * \left(6 - \left(1.77 - 0.42x \frac{(\ln TP)}{\ln 2} \right) \right) \quad (2)$$

Lamparelli [26] considers six different levels of trophic status: ultraoligotrophic ($IET-(TP) \leq 47$), oligotrophic ($47 < IET-(TP) \leq 52$), mesotrophic ($52 < IET-(TP) \leq 59$), eutrophic ($59 < IET-(TP) \leq 63$), super-eutrophic ($63 < IET-(TP) \leq 67$), and hypereutrophic ($IET-(TP) > 67$), where the first level corresponds to clean water and the subsequent levels represent increasing eutrophication.

The chemical parameters of water quality (TP, TN, estimated Chl-a*), and the reservoir trophic level index (RTLI-(TP)), were used as a reference to analyze the spectral information and, furthermore, working as a tool for the definition of a possible pollution spectral signature for the 29 April 2022, using the closest monitoring day, the 27 April 2022.

2.3.3. Water Characteristics Modeling

Vegetation, soil, and water have typical spectral reflectance curves (Figure 4a) allowing to differentiate these types of land cover by remote sensing techniques [33]. Thus, these distinctive spectral signatures support the use of various spectral indices and bands ratios to monitor vegetation and water by remote sensing [8]. In this study the spectral indices NDWI, NDVI, and the B/G ratio were considered for water quality parameters estimation using remote sensing techniques. The interpretation of the NDVI, NDWI, and B/G ratio was very straightforward in the light of the reflectance curves presented in Figure 4, the formulas in Table 3, and values range provide in Section 2.3.1.

Spectral bands, spectral indices, and band ratios provide information on several water quality parameters associated with optically active constituents [8–12], specifically: dissolved oxygen (DO), total phosphorus (TP), total suspended solids (TSSs), turbidity (TUR), and chlorophyll-a (Chl-a) (Table 4).

The 13 optical water types for inland waters, derived from hyperspectral water reflectance measurements, were used as a proxy for the analysis of the spectral bands' image ratio (B/G) (Figure 4b), as described by Spyarakos et al. [34].

Based on the analysis of spectral indices conducted from October 2021 to January 2023 (NDWI, NDVI, and B/G), the 29 May 2022 was selected as it showed the highest variability. The defined spectral signatures correspond to five water classes, as follows: 1—deep water, 2—shallow water, 3—eutrophic water, 4—median deep water, and 5—turbid water. Nine spectral bands with a spatial resolution of 20 m (B, G, R, R-edge 1, R-edge 2, R-edge 3, NIR narrow, SWIR1, and SWIR2; (Table 1) were used for classification and modeling purposes. The FCC, NDWI, NDVI, and B/G ratios were computed using the 20 m imagery. A water mask grid was used to extract the Marateca reservoir. Principal component analysis (PCA) was used for dimensionality reduction, where the first factor explains more than 95% of the data's variability. A false-color composite was generated using the B/G ratio, NDVI, and NDWI imagery and an unsupervised procedure.

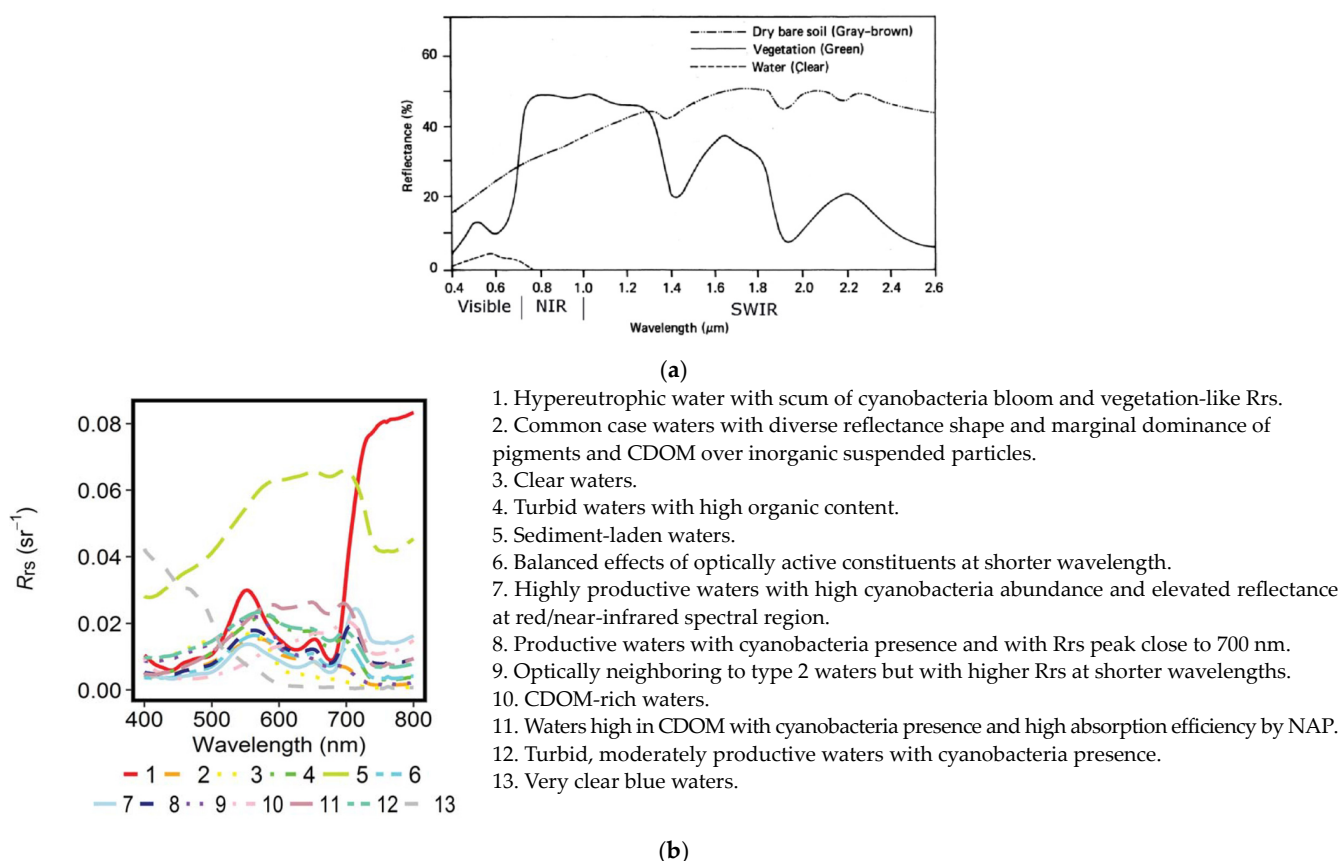


Figure 4. Reflectance curves: (a) clear water, green vegetation and dry bare soil by Lillesand and Kiefer [33]; and (b) optical water types by Spyarakos et al. [34].

Table 4. Water quality parameters with optical active constituents measured by remote sensing [8–12].

Acronym	TP	Chl-a	TSS	TUR	DO
NDVI		x			
B/G	x	x	x	x	x

TP—total phosphorus, Chl-a—chlorophyll, TSS—total suspended solids, TUR—turbidity and DO—dissolved oxygen.

The K-means cluster analysis for grids was used to define the natural spectral classes in the imagery, using four, five, and ten clusters, correspondingly. Furthermore, a supervised classification was conducted based on this initial exploratory analysis and ground-truth knowledge supported by the water quality parameters measured in the Marateca reservoir monitoring points. The first step of the supervised classification involved the definition of training areas as a reference to generate class signatures, using the nine spectral bands. The water quality classes considered were as follows: 1—deep water, 2—shallow water, 3—eutrophic water, 4—median deep water, and 5—turbid water. The second step involved using classifier algorithms (such as the maximum likelihood—MaxLike) to classify the entire image into the spectral classes previously identified.

The random forest algorithm (ML-RF) was used as a machine learning procedure, using the previously defined training areas, on the 30 March 2022 (pre-event), the 29 April 2022 (post-event), and the 29 May 2022 (post-event). An error matrix was computed to assess the quality of the obtained results for the training areas for the different tested approaches. The land cover category on the training subset (ground truth) and the classification results for the same location us allowed to quantify the percentage of correctly classified pixels, and the Kappa coefficient was used to quantify the model's accuracy [35].

3. Results

3.1. Composites, Spectral Indices, Ratios Imagery and Spectral Signatures

The FCC, NDWI, NDVI, and B/G ratio imagery (with a spatial resolution of 10 m) for the dates of 30 March 2022 (pre-event), 29 April 2022 (post-event 1), and 29 May 2022 (post-event 2) revealed certain patterns. In March, the land cover exhibited high humidity due to the significant precipitation that occurred during that month (Figures 2a and 5a). An observed plume entering at point P5 was noticeable in both the DNWI and B/G ratio images (Figure 5b,d).

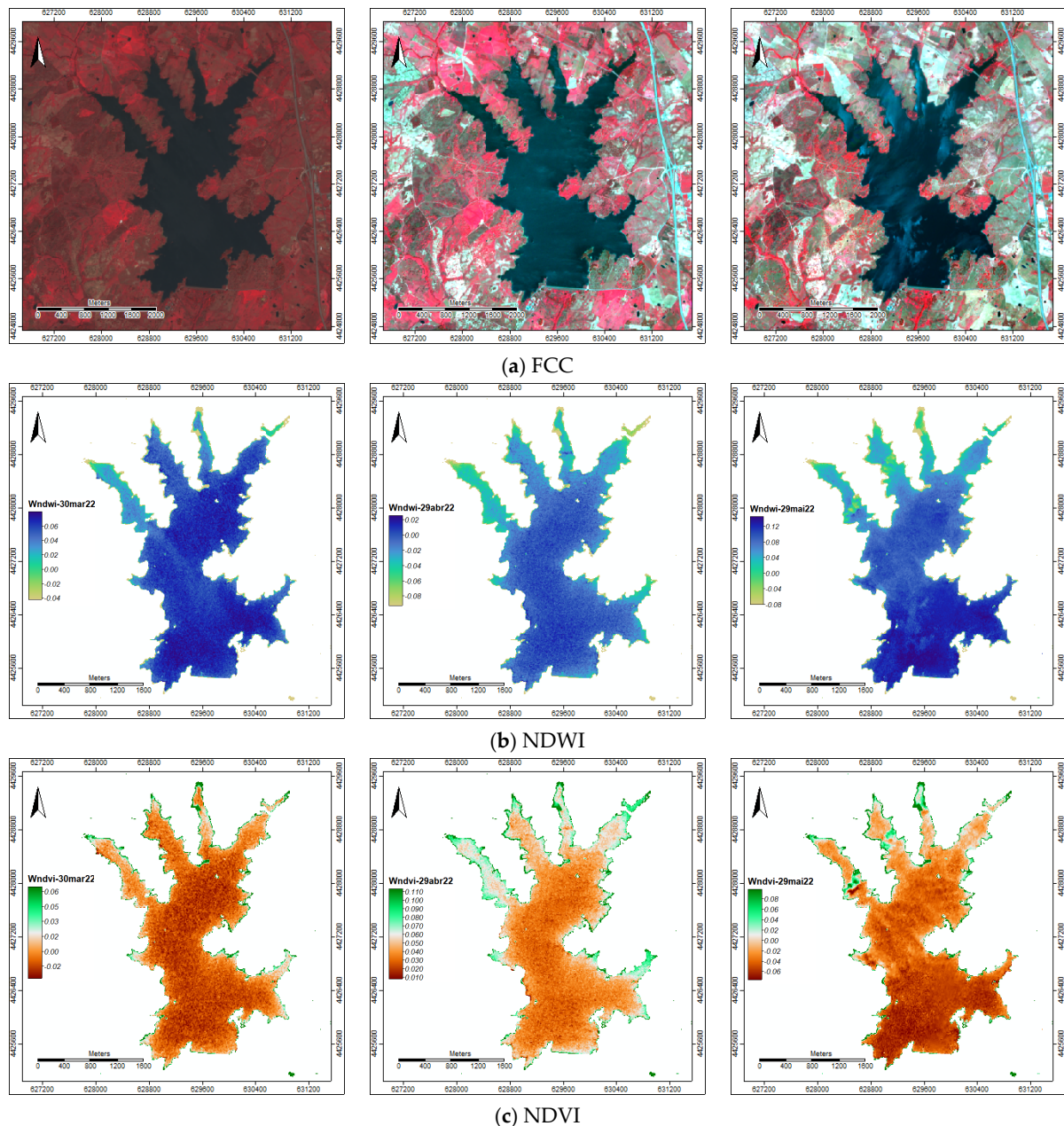


Figure 5. Cont.

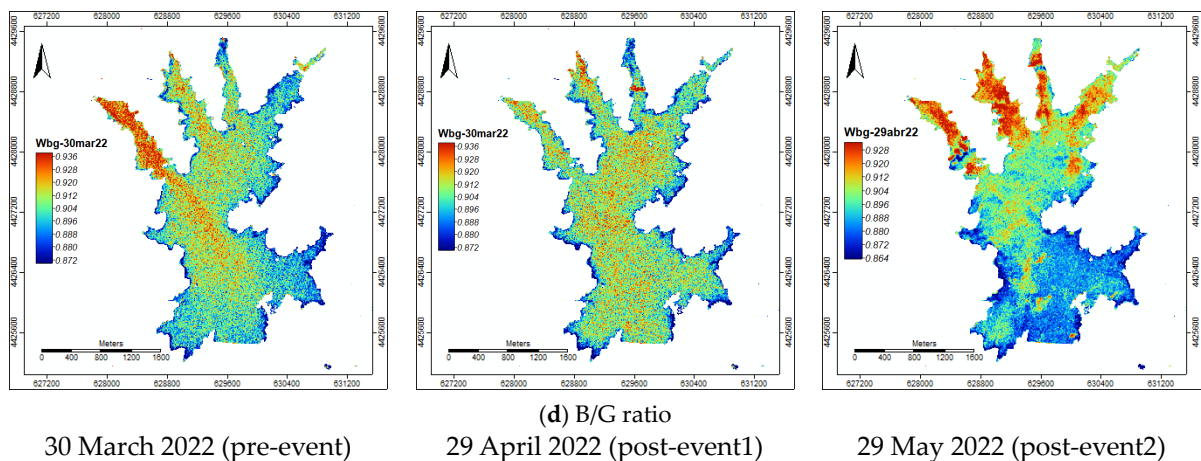


Figure 5. Study area—Marateca reservoir imagery (10 m spatial resolution) for the dates of 30 March 2022, 29 April 2022, and 29 May 2022: (a) FCC; (b) NDWI; (c) NDVI; and (d) B/G ratio.

The monthly difference indices dNDWI and dNDVI, calculated between the 30th of March 2022 (pre-event), the 29 April 2022 (post-event 1), and the 29 May 2022 (post-event 2), further emphasized the observed changes (Figure 6). These indices highlighted the impact of the weather conditions during this period, with intense precipitation in March followed by significantly reduced precipitation in April and May (Figure 2a). As a result, any contamination or pollutants had less dilution due to the limited rainfall during the later months.

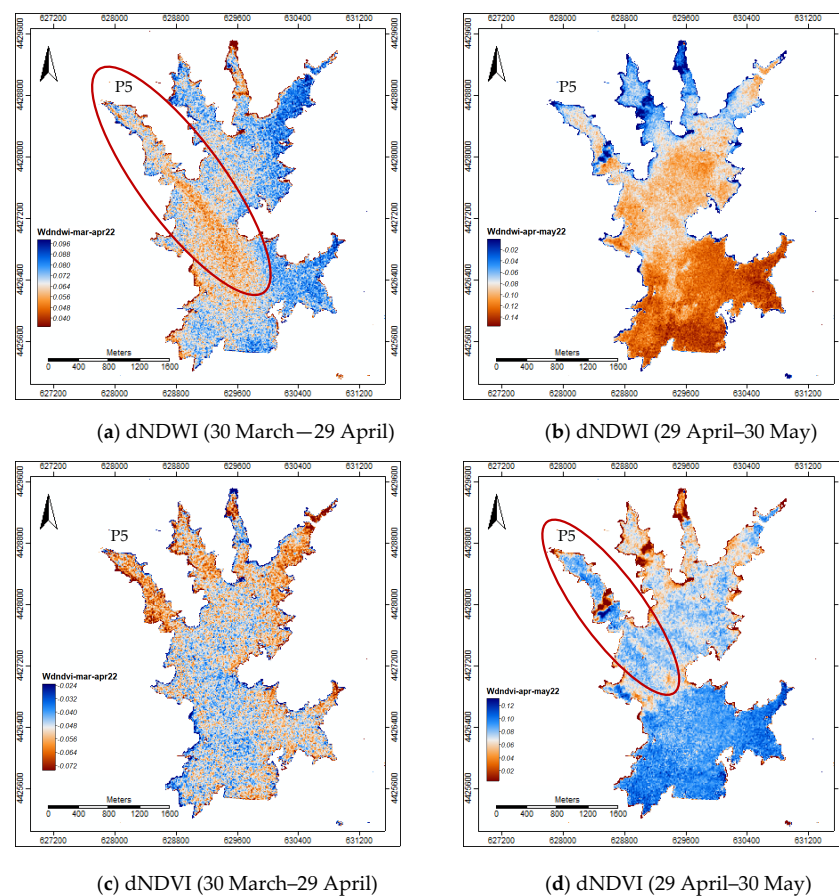


Figure 6. Study area—Marateca indices change: (a) dNDWI (30 March–29 April); (b) dNDWI (29 April–30 May); (c) dNDVI (30 March–29 April); and (d) dNDVI (29 April–30 May).

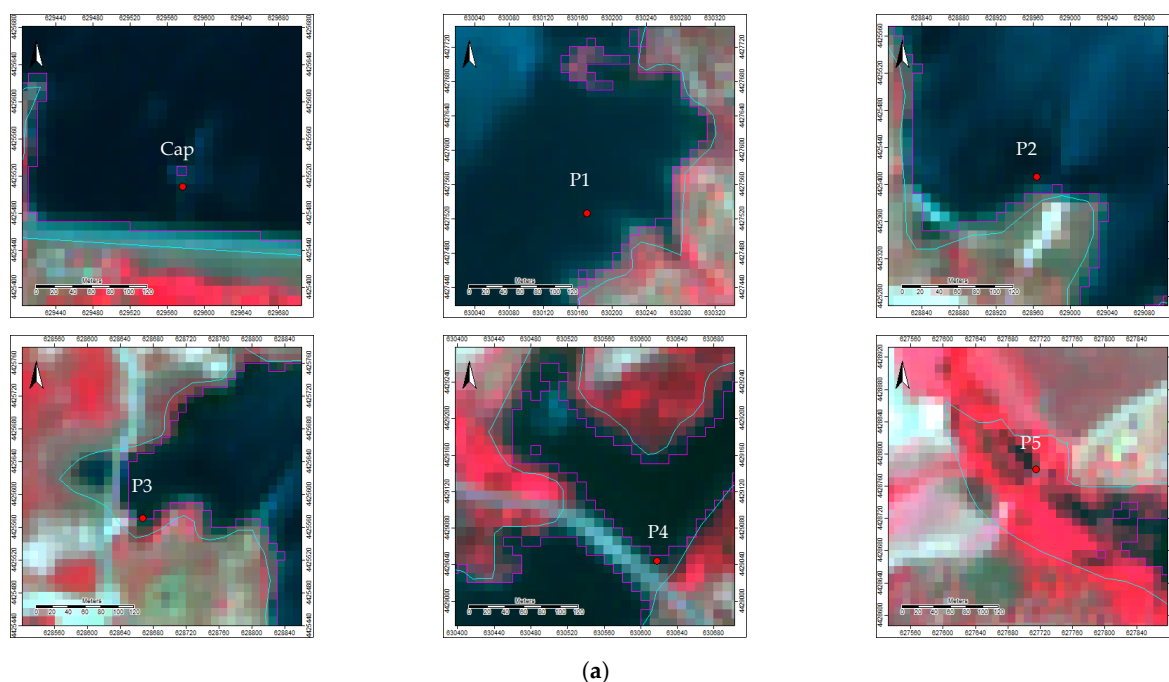
Overall, comparing the pre-event and post-event 1 periods, the dNDWI exhibited positive values, indicating an increase in moisture content. However, a noticeable plume was observed at the entry point P5 (Figure 6a—highlighted in red). Between the post-event 1 and post-event 2 periods, negative values were observed in the dNDWI (Figure 6b), indicating a decrease in moisture content.

On the other hand, the dNDVI showed negative values between the pre-event and post-event 1 period (Figure 6c), suggesting a decrease in eutrophication, particularly at the east side of the reservoir and the water entry points. This decrease could be attributed to the high precipitation that occurred in March (Figure 2a). Between the post-event 1 and post-event 2 periods, positive values were observed in the dNDVI indicating an increase in eutrophication, primarily at the entry point P5 (Figure 6d—highlighted in red).

The spectral reflectance signatures in the monitoring points location (Figure 1b) were obtained with the sole purpose of exploring and validating the measurements in situ by APA. The multispectral imagery of 20 m spatial resolution, as nine bands were available (Table 1), provided a more complete spectral reflectance signature along the electromagnetic spectrum. Despite monitoring points sensors being in the water, mixed pixels of water and surrounding vegetation, bare soil, and infrastructures were observed in the 20 m spatial resolution imagery (e.g., Cap, P4, and P5) (Figure 7a). The spectral signatures obtained from the monitoring points locations on 30 March 2022 (pre-event), 29 April 2022 (post-event 1), and 29 May 2022 (post-event 2) demonstrated a general trend of increasing differentiation between the monitoring points locations (Figure 7b) as no precipitation occurred in April and May (Figure 2a). The effect of mixed pixels is more evident from Cap, P1, P2, P4, P3 to P5 monitoring point locations, with the latter showing a reflectance curve like the vegetation reflectance curve (see Figure 4a).

3.2. Water Quality Parameters—Monitoring and Validation Data

The Capt monitoring point was the only point with consistent continuous data collection from October to April 2022. On the 8 March 2022 (pre-event), the Capt point had very high values for the parameters TP, TN, and Chl-a and moderate values for TSS and TUR (Figure 8). On the 10 April 2022, a significant number of dead fish in the reservoir were observed.



Blue line—reservoir limit by COS2018; and purple line—reservoir limit by single band extraction.

Figure 7. Cont.

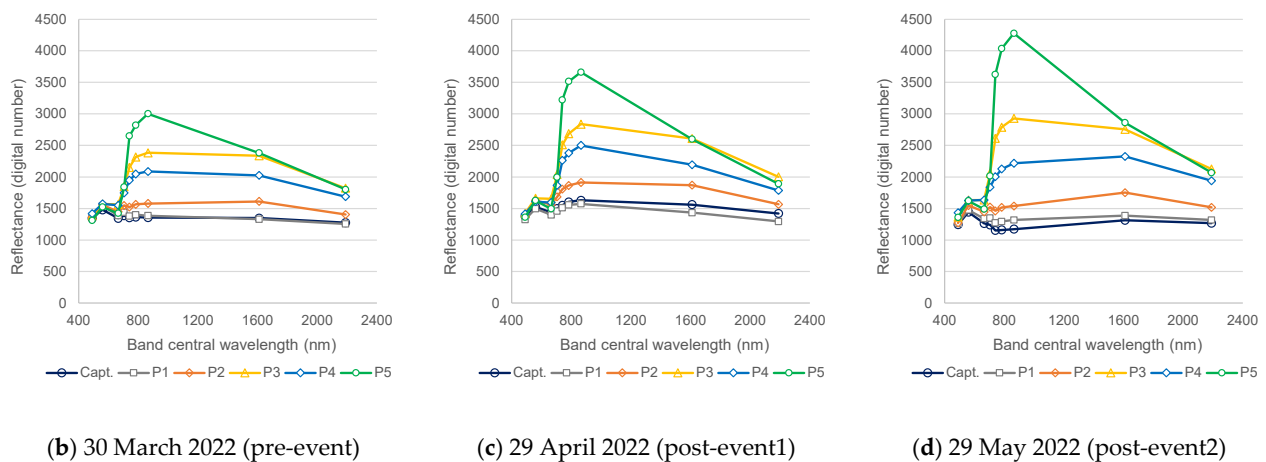


Figure 7. Study area—Marateca reflectance curves for the monitoring points: (a) monitoring points Capt, P1, P2, P3, P4, and P5 over the FCC 29 May 2022; (b) reflectance curves 30 March 2022 (pre-event); (c) reflectance curves 29 April 2022 (post-event); and (d) reflectance curves 29 May 2022 (post-event).

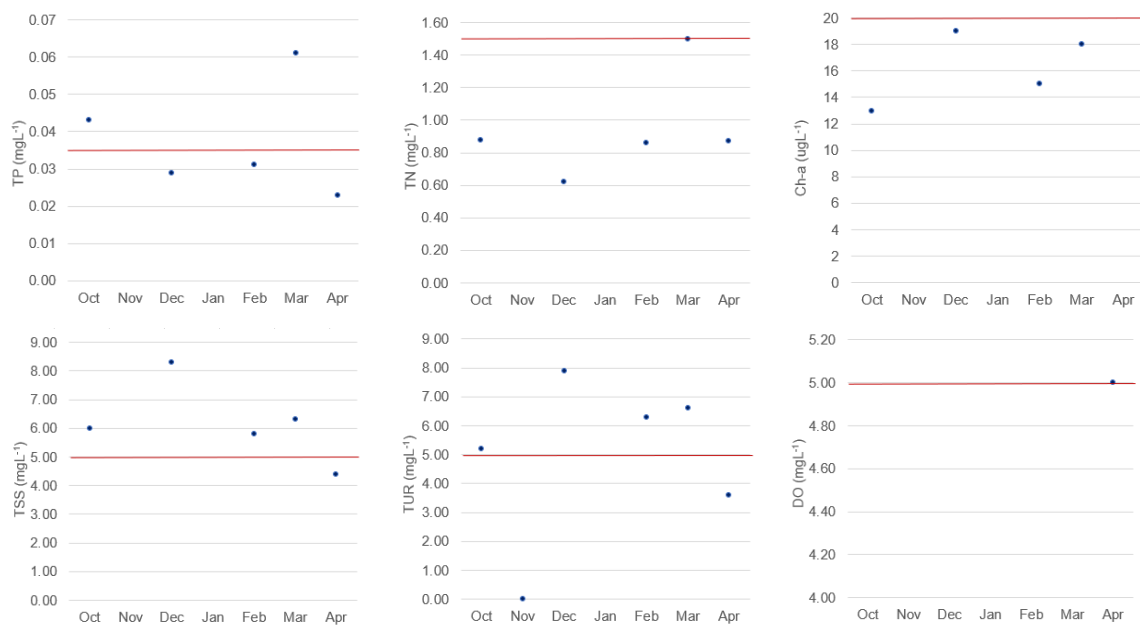


Figure 8. Study area—Marateca's water quality parameters at the monitoring sampling point Capt from October 2021 to April 2022 and maximum admissible values (red line): TP—total phosphorus, TN—total nitrogen, Chl-a—chlorophyll, TSS—total suspended solids, TUR—turbidity, and DO—dissolved oxygen.

The Capt monitoring point was the only location with continuous data collection available from October to April 2022. On 8 March 2022 (pre-event), the Capt point exhibited extremely high values for TP, TN, and Chl-a, along with moderate values for TSS and TUR (Figure 8). This indicates a potentially high nutrient load and algal biomass in the reservoir. On 10 April 2022, a significant occurrence of dead fish in the reservoir was observed, indicating a possible adverse event.

On 27 April 2022 (post-event 1), water quality parameters for TP and TN were available for most of the monitoring points, including Capt, P1, P3, P4, and P5. These parameters were the focus of the analysis in this study for validation purposes (Figure 9).

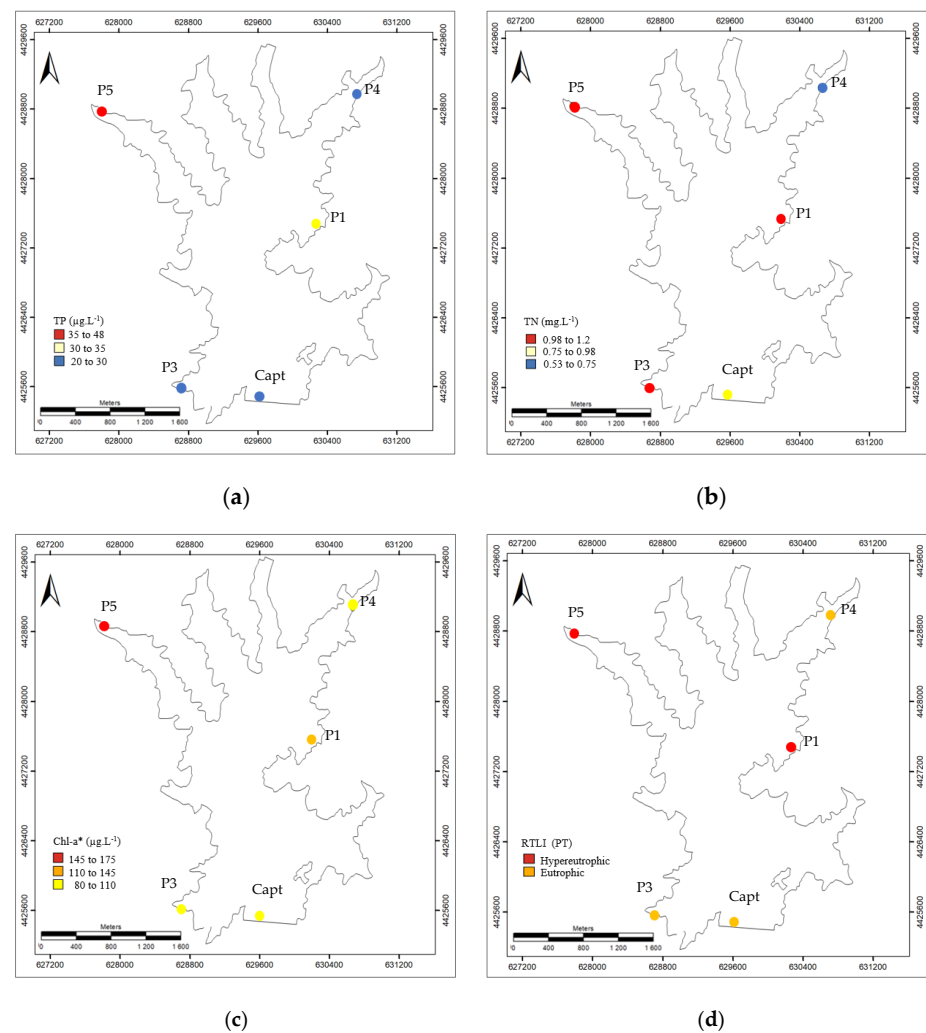


Figure 9. Values at monitoring points (Capt, P1, P3, P4 and P5) on 27 April 2022 (post-event) for: (a) TP—total phosphorus, (b) TN—total nitrogen, (c) Chl-a*—estimated chlorophyll-a, and (d) RTLI (TP)—reservoir trophic level index [26].

The evaluation of the obtained values for the five monitoring points (Capt, P1, P3, P4, and P5) concerning the maximum admissible value for TP, which is $35 \mu\text{g L}^{-1}$ according to DL n°152/2017, 7 December 2017 [36], showed that point P5 had high TP values, point P1 had intermediate values, while points Capt, P3, and P4 had low TP values (Figure 9a).

Regarding TN (total nitrogen), when considering the maximum allowable value of 1.5 mg L^{-1} according to DL n°152/2017, dated 7 December 2017 [36], elevated levels were observed at points P1, P3, and P5, an intermediate level at Capt, and a lower level at P4. Notably, point P5 displayed the highest values for both TP (total phosphorus) and TN, surpassing the allowable maximum allowable values (Figure 9b). Regarding the estimated values of Chl-a*, and assuming the allowable value of $20 \mu\text{g L}^{-1}$ for reservoirs by the Portuguese Environmental Agency (APA), it is evident that the distribution aligns with the TP values and surpasses the allowable threshold in all monitoring points.

The reservoir's trophic level index (RTLI-(TP)), measured in the gauging stations revealed two levels [26]: a Hypereutrophic level at points P1 and P5, and a Eutrophic level at Capt, P3, and P4, indicating that corrective actions are needed (Figure 9c).

The defined spectral signatures for the gauging stations on 29 April 2022 (Figure 7b), were consistent with the water quality chemical parameters TP, TN, and estimated Chl-a*, as well as the reservoir trophic level index (RTLI-(TP)) on the 27 April 2022 (Figure 8). Indeed, point P5 showed a spectral signature pattern that closely resembled the curve for

the Hypereutrophic water type, which is consistent with the trophic level computed using the chemical contents of the selected covariates collected in the same day (Figure 4).

3.3. Water Characteristics Modeling

The imagery for the 29 May 2022 (Figure 5) showed to have the highest variability in water characteristics throughout this reservoir when compared to the 30 March and the 29 April 2022. The spectral signatures at the monitoring points also appeared to have less spectral confusion on 29 May 2022 (Figure 7c). This variability was also highlighted by the first principal component image and the false-color composite image from the B/G ratio, NDVI, and NDWI imagery (Figure 10a,b).

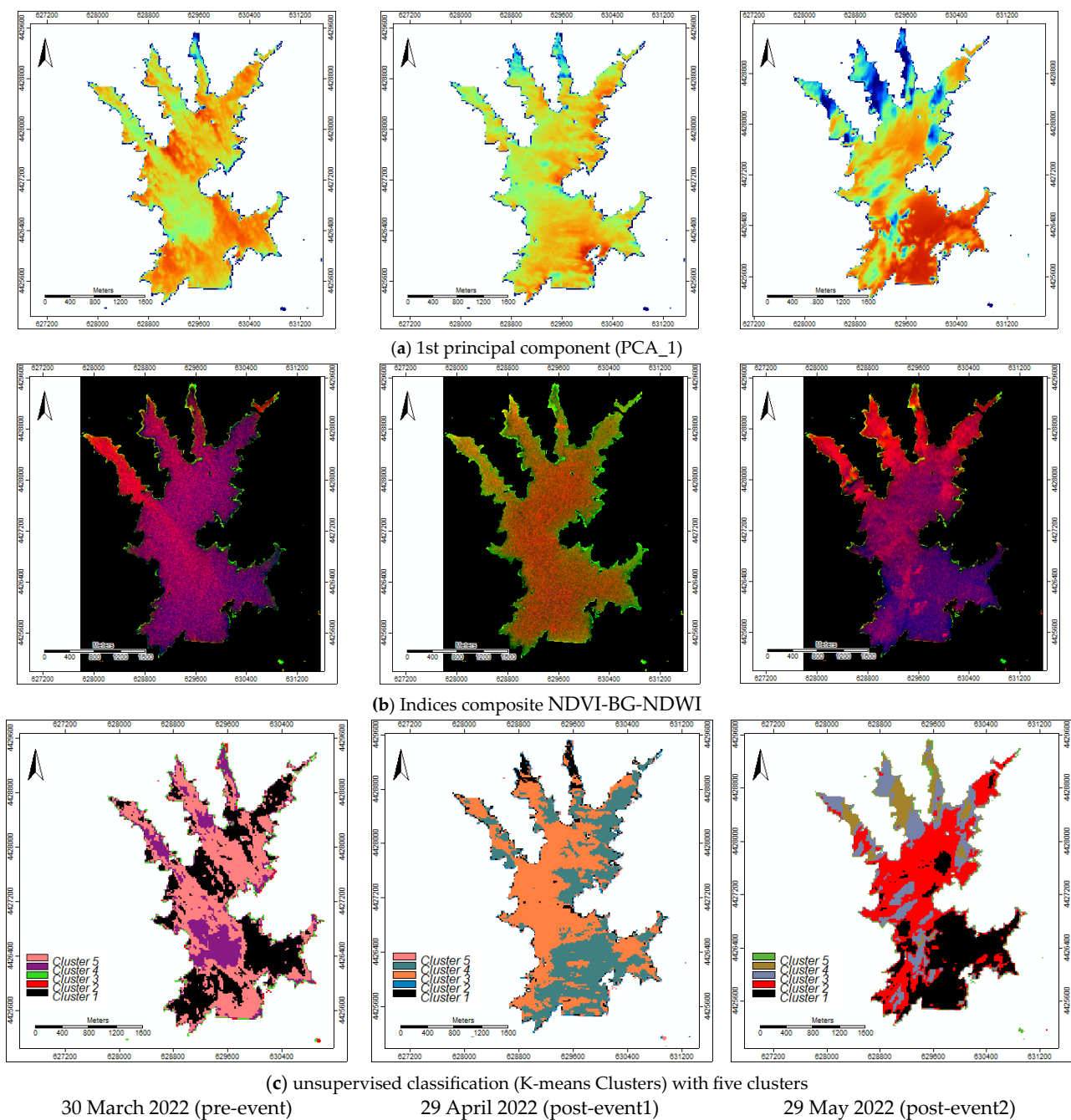


Figure 10. Study area—Marateca reservoir imagery (20 m spatial resolution) for the dates of 30 March 2022, 29 April 2022, and 29 May 2022: (a) 1st principal component (PCA_1); (b) indices composite NDVI-BG-NDWI; and (c) unsupervised classification (K-means Clusters) with five clusters.

The nine spectral bands (e.g., B, G, R, R-edge 1, R-edge 1, R-edge 1, NIR narrow, SWIR1, and SWIR2) natural clustering with four, five, and ten clusters obtained by the unsupervised procedure (e.g., K-means cluster analysis for grids) also emphasized the variability previously observed and highlighted possible training areas with no spectral confusion (Figure 10c).

Based on the unsupervised clustering image and the ground-truth knowledge, supported by the Marateca reservoir monitoring points water quality chemical parameters data, the digitalized training areas (polygons) for five water characteristics classes considered (e.g., 1—deep water; 2—shallow water; 3—eutrophic water; 4—median deep water; and 5—turbid water) again revealed that its spectral signatures had no spectral confusion (Figure 11).

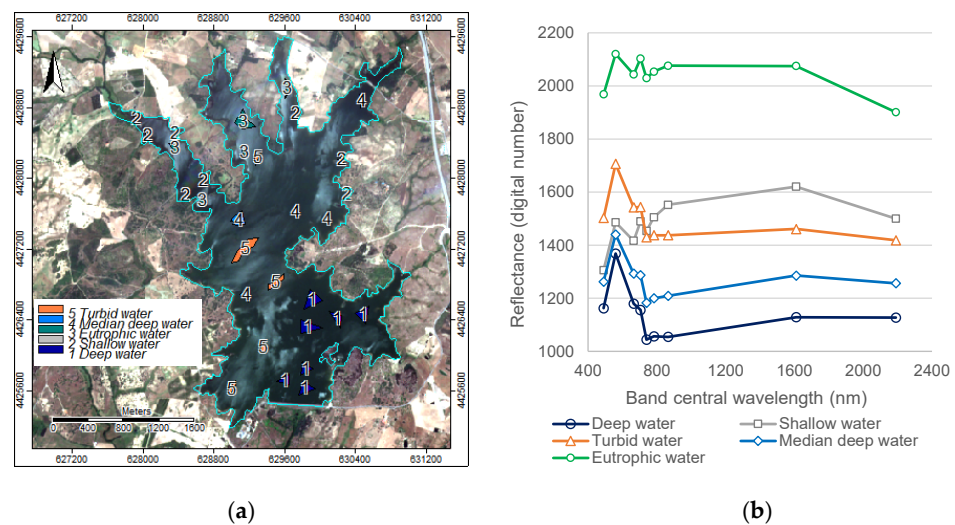


Figure 11. Study area—Marateca reservoir reflectance curves on 29 May 2022 imagery of 20 m spatial resolution: (a) training areas (polygons); and (b) reflectance curves for the considered five water classes (e.g., 1—deep water; 2—shallow water; 3—eutrophic water; 4—median deep water; and 5—turbid water).

The imagery taken on 29 May 2022 (Figure 5) exhibited the highest variability in water characteristics within the reservoir compared to the images taken on 30 March and 29 April 2022. The spectral signatures at the monitoring points also showed less spectral confusion on 29 May 2022 (Figure 7c). This variability was further highlighted by the first principal component image and the false-color composite image derived from the B/G ratio, NDVI, and NDWI imagery (Figure 10a,b).

The natural clustering of the nine spectral bands (B, G, R, R-edge 1, R-edge 1, R-edge 1, NIR narrow, SWIR1, and SWIR2) using unsupervised clustering techniques such as K-means cluster analysis with four, five, and ten clusters emphasized the observed variability and identified potential training areas with minimal spectral confusion (Figure 10c).

Based on the unsupervised clustering image and the ground-truth information provided by the water quality chemical parameters from the Marateca reservoir monitoring points, the digitalized training areas (polygons) for the five water characteristic classes (deep water, shallow water, eutrophic water, median deep water, and turbid water) demonstrated once again that their spectral signatures were distinct without spectral confusion (Figure 11).

The error matrix computed to validate the training areas (Figure 11a) against the classified image by the classifier of the maximum likelihood (MaxLike) delivered an overall accuracy and a Cohen's Kappa coefficient of 99%. The error matrix between the Maxlike image and the Cluster 5 image (Figure 10c) delivered an overall accuracy of 72% and a Cohen's Kappa coefficient of 45%.

The error matrix between the ML-RF simulated image (Figure 12b), modeled using the training areas (Figure 11a), and the Cluster 5 image (Figure 10c) delivered an overall accuracy of 76% and a Cohen's Kappa coefficient of 53%. The ML-RF simulated images for the 30 March 2022, 29 April 2022, and the 30 May (Figure 12), using the training areas digitalized on the 29 May 2022 (Figure 11a), clearly identified the natural clusters (Figure 10c), particularly the plume at the entry point P5 and the eutrophication zones (Figures 5 and 6).

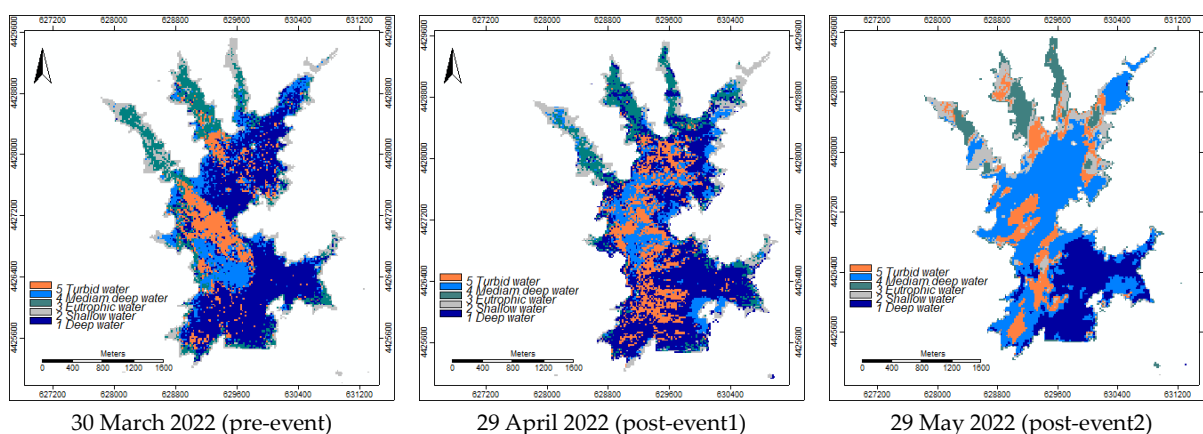


Figure 12. Study area—Marateca reservoir imagery modeling by ML-RF for: (a) 30 March 2022; (b) 29 April 2022; and (c) 29 May 2022.

The error matrix was computed to validate the training areas (Figure 11a) by comparing them against the classified image generated by the maximum likelihood (MaxLike) classifier. The overall accuracy of the classification was found to be 99%, indicating a high level of agreement between the classified image and the training areas. The Cohen's Kappa coefficient, which quantifies the model accuracy beyond random chance, was also 99%.

When comparing the MaxLike classified image with the Cluster 5 image (Figure 10c), the overall accuracy was 72% with a Cohen's Kappa coefficient of 45%. This indicates a moderate level of agreement between the two images.

Similarly, when comparing the ML-RF simulated image (Figure 12b), generated using the training areas from Figure 11a, with the Cluster 5 image (Figure 10c), the overall accuracy was 76% with a Cohen's Kappa coefficient of 53%. This suggests a moderate level of agreement between the ML-RF simulated image and the Cluster 5 image.

The ML-RF simulated images for 30 March 2022, 29 April 2022, and 30 May 2022 (Figure 12), which were generated using the training areas digitalized on 29 May 2022 (Figure 11a), successfully identified the natural clusters observed in Figure 10c. Specifically, the plume at the entry point P5 and the eutrophication zones, as depicted in Figures 5 and 6, were identified in the ML-RF simulated images.

4. Discussion and Conclusions

Spectral information obtained from measurement points plays a vital role in understanding the ecological dynamics of water bodies, particularly in relation to trophic levels. By validating spectral signatures at these measurement points, it becomes possible to estimate trophic levels continuously and comprehensively throughout the entire reservoir. In the context of reservoirs and aquatic ecosystems, different trophic levels, ranging from oligotrophic (low nutrient levels) to hypereutrophic (high nutrient levels), exhibit distinct spectral signatures. These signatures are essential for assessing the overall health and productivity of the ecosystem. By conducting thorough validation of the spectral information collected at measurement points, it is possible to assume the corresponding spectral signatures. This validation process involves rigorous analysis and comparison of the obtained data with established reference data (gauging points), ensuring accuracy and consistency.

Once the spectral signatures are validated, they can be used to estimate trophic levels continuously and across the entire reservoir. Further work will include the integration of more sensors strategically positioned in a uniform grid over the entire reservoir area. This approach will facilitate the application of advanced interpolation techniques, enabling the creation of a trophic level's estimated mapping that after can be overlayed onto the patterns acquired through remote sensing, and, consequently, enabling a more precise validation of the spectral signatures.

Continuous estimation of trophic levels is a significant advancement in environmental monitoring. It allows for real-time tracking of changes in nutrient levels and overall ecological conditions. This information is crucial for identifying potential sources of pollution, understanding the impact of human activities on the ecosystem, and implementing timely and targeted remediation measure. Furthermore, continuous trophic level estimation provides a comprehensive and holistic view of the reservoir's health. It enables environmental authorities and policymakers to identify critical areas of concern and allocate resources effectively to protect and preserve the water body. Moreover, such data-driven approaches can guide sustainable management practices to maintain a balanced and thriving ecosystem.

Concerning the Marateca reservoir, the conducted survey allowed for the identification of two trophic index levels (RTLI-(TP)) [26] which showed two levels: the hypereutrophic level at points P1, P2, and P5 and the eutrophic level at points Capt, P3, and P4, and confirming entry point P5 as one of the most problematic. Indeed, the principal sources of nutrients in lakes and reservoirs are land runoff and atmospheric inputs. Relatively small internal reservoirs, such as Marateca, are highly sensitive to seasonal intakes. Runoff and atmospheric inputs may vary significantly in the concentration and ratio of TP and TN, and, therefore, in the proportion of organic and inorganic forms of these nutrients [37,38]. Two reasons that may explain the elevated levels of TP, TN, and estimated Chl-a. One possibility is eutrophication due to agricultural fertilizers. In this scenario, a high TP value and a lower TN value would be expected. The second possibility is soil erosion with the transport of large amounts of nutrients into the reservoir, especially phosphorus which tends to adhere to soil particles, while nitrogen is more soluble can be washed away more easily [39,40]. Furthermore, the identified hypereutrophic and eutrophic levels refer to excessive growth of algae and other aquatic plants in the water body. This growth is often caused by an excess of nutrients such as phosphorus and nitrogen in the water. When these nutrients are available in abundance algae and other plants can grow very quickly, leading to the water body becoming overgrown and appearing green or brown. This excess growth of plants can also lead to a depletion of oxygen in the water, which can harm fish and other aquatic life, and is often the result of human activities such as agriculture, urbanization, and industrialization. Due to the high precipitation in March, an increase in moisture content, particularly at the east side of the reservoir, was observed along with a decrease in eutrophication also at the east side and mostly at the reservoir water entries. During the following two months, there was no significant precipitation, consequently, a decrease in moisture content and an increase in eutrophication occurred, mostly at entry point P5.

In this study, five water characteristics classes were differentiated in the Marateca reservoir (e.g., 1—deep water; 2—shallow water; 3—eutrophic water; 4—median deep water; and 5—turbid water) using the spectral signatures created with the 29 May 2022 imagery. The ML-RF simulated image, modeled using these training areas, delivered an overall accuracy of 76% and a Cohen's Kappa coefficient of 53% when compared to the Cluster 5 image (natural clustering) proving to be robust. Thus, these training areas allowed modeling of the Marateca reservoir water characteristics for the period under analysis (March, April, and May 202) forecasting the problematic zones either due to drought and/or contamination. The Sentinel2A imagery proved to be a valuable monitoring tool, as the spectral information aligns with the point measured data, allowing validation of the nominal spectral signatures for TP, TN, and Chl-a*. The reservoir's continuous water quality evaluation in conjunction with traditional sampling methods and field surveying for validation is a promising approach for pollution control [8–12].

The methodological approach developed in this study can be easily applied to other reservoirs and is a key support tool for decision-makers. Nevertheless, continuous monitoring with consistent data collection over time is mandatory. Furthermore, the water sample's location should be improved to provide a better distribution of water quality parameters throughout the entire reservoir for effective variability monitoring.

Author Contributions: Conceptualization, C.A.; data curation, C.A. and T.A.; methodology, C.A. and T.A.; formal analysis, writing—original draft preparation, C.A. and T.A.; writing—review and editing, C.A. and T.A. All authors have read and agreed to the published version of the manuscript.

Funding: This study was funded by CERNAS-IPCB [UIDB/00681/2020] funding from the Foundation for Science and Technology (Fundação para a Ciência e Tecnologia—FCT); and by ICT [UIDB/04683/2020] also funding from FCT.

Institutional Review Board Statement: Not applicable.

Informed Consent Statement: Not applicable.

Data Availability Statement: The datasets used in this survey were downloaded from public databases.

Conflicts of Interest: The author declares no conflict of interest.

Appendix A

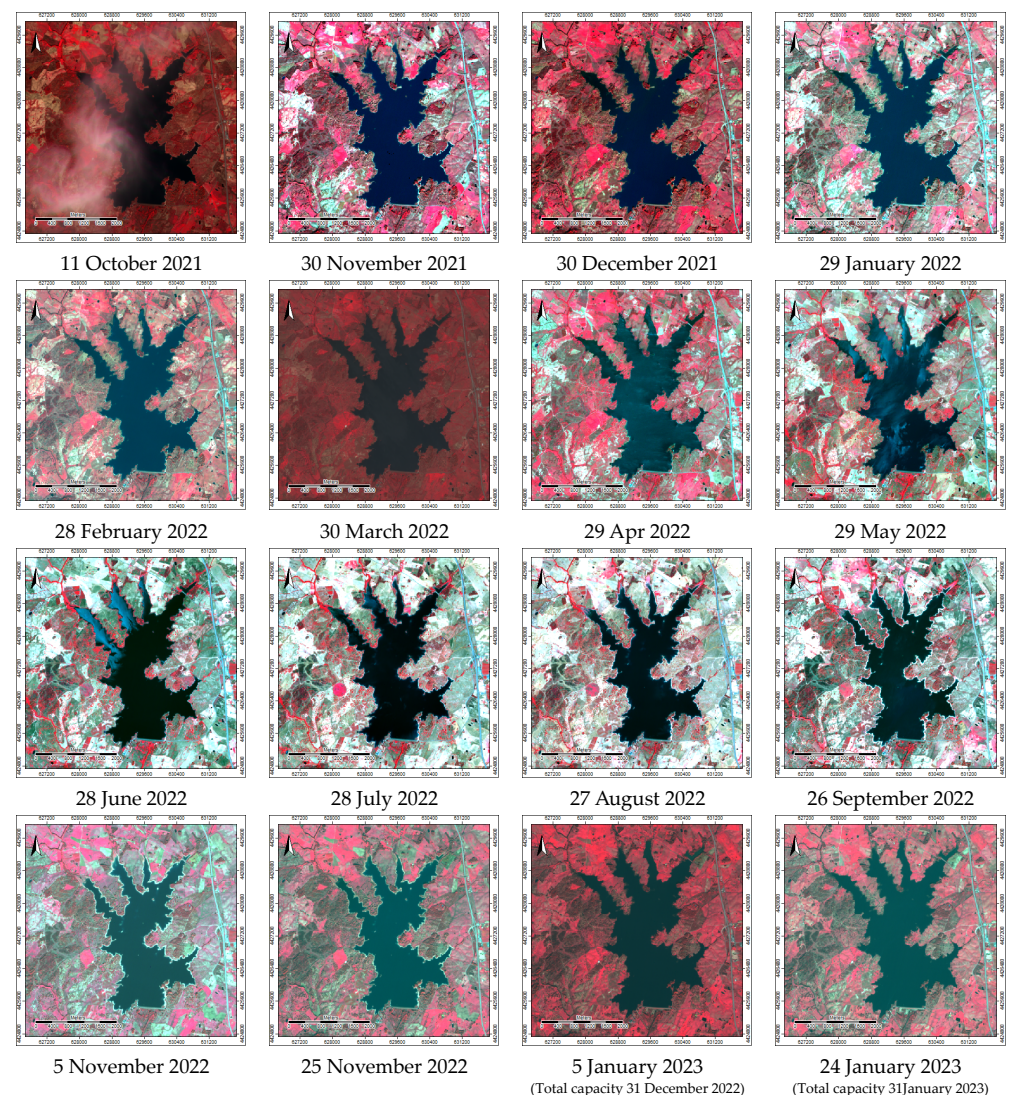


Figure A1. Study area—Marateca reservoir: FCC imagery (October 2021 to January 2023).

References

1. Makanda, K.; Nzama, S.; Kanyerere, T. Assessing the role of water resources protection practice for sustainable water resources management: A Review. *Water* **2022**, *14*, 3153. [CrossRef]
2. Russo, T.; Alfredo, K.; Fisher, J. Sustainable water management in urban, agricultural, and natural systems. *Water* **2014**, *6*, 3934–3956. [CrossRef]
3. Zaghloul, A.; Saber, M.; Gadow, S.; Awad, F. Biological indicators for pollution detection in terrestrial and aquatic ecosystems. *Bull. Natl. Res. Cent.* **2020**, *44*, 127. [CrossRef]
4. Saad Abdelkarim, M. Biomonitoring and bioassessment of running water quality in developing countries: A case study from Egypt. *Egypt. J. Aquat. Res.* **2020**, *46*, 313–324. [CrossRef]
5. El-Serehy, H.A.; Abdallah, H.S.; Al-Misned, F.A.; Irshad, R.; Al-Farraj, S.A.; Almalki, E.S. Aquatic ecosystem health and trophic status classification of the Bitter Lakes along the main connecting link between the Red Sea and the Mediterranean. *Saudi J. Biol. Sci.* **2018**, *25*, 204–212. [CrossRef]
6. Zaghloul, A.; Saber, M.; Abd-El-Hady, M. Physical indicators for pollution detection in terrestrial and aquatic ecosystems. *Bull. Natl. Res. Cent.* **2019**, *43*, 120. [CrossRef]
7. Zaghloul, A.; Saber, M.; El-Dewany, C. Chemical indicators for pollution detection in terrestrial and aquatic ecosystems. *Bull. Natl. Res. Cent.* **2019**, *43*, 156. [CrossRef]
8. Gholizadeh, M.H.; Melesse, A.M.; Reddi, L. A comprehensive review on water quality parameters estimation using remote sensing techniques. *Sensors* **2016**, *16*, 1298. [CrossRef]
9. Cabezas-alzate, D.F.; Garcés, Y.A.; Henao-cespedes, V. LANDSAT-7 ETM+ based remote sensing as a tool for assessing lakes water quality characteristics. *J. Southwest Jiaotong Univ.* **2021**, *56*, 291–301. [CrossRef]
10. Warren, M.A.; Simis, S.G.H.; Selmes, N. Complementary water quality observations from high and medium resolution Sentinel sensors by aligning chlorophyll-a and turbidity algorithms. *Remote Sens. Environ.* **2021**, *265*, 112651. [CrossRef]
11. Chu, H.J.; He, Y.C.; Chusnah, W.N.; Jaelani, L.M.; Chang, C.H. Multi-reservoir water quality mapping from remote sensing using spatial regression. *Sustainability* **2021**, *13*, 6416. [CrossRef]
12. Li, X.; Ding, J.; Ilyas, N. Machine learning method for quick identification of water quality index (WQI) based on Sentinel-2 MSI data: Ebinur Lake case study. *Water Sci. Technol. Water Supply* **2021**, *21*, 1291–1312. [CrossRef]
13. Yang, H.; Kong, J.; Hu, H.; Du, Y.; Gao, M.; Chen, F. A review of remote sensing for water quality retrieval: Progress and challenges. *Remote Sens.* **2022**, *14*, 1770. [CrossRef]
14. Shafique, A.; Cao, G.; Khan, Z.; Asad, M.; Aslam, M. Deep learning-based change detection in remote sensing images: A review. *Remote Sens.* **2022**, *14*, 871. [CrossRef]
15. Gwon, Y.; Kim, D.; You, H.; Nam, S.H.; Kim, Y. A standardized procedure to build a spectral library for hazardous chemicals mixed in river flow using hyperspectral image. *Remote Sens.* **2023**, *15*, 477. [CrossRef]
16. Bria, A.; Cerro, G.; Ferdinandi, M.; Marrocco, C.; Molinara, M. An IoT-ready solution for automated recognition of water contaminants. *Pattern Recognit. Lett.* **2020**, *135*, 188–195. [CrossRef]
17. Miranda, P.M.A.; Coelho, F.E.S.; Tomé, A.R.; Valente, M.A.; Carvalho, A.; Pires, C.; Pires, H.O.; Pires, V.C.; Ramalho, C. 20th Century Portuguese Climate and Climate Scenarios. In *Climate Change in Portugal: Scenarios, Impacts and Adaptation Measures (SIAM Project)*; Santos, F.D., Forbes, K., Moita, R., Eds.; Gradiva: Lisbon, Portugal, 2002; pp. 23–38.
18. APA. Barragem da Marateca. Comissão Nacional Portuguesa das Grandes Barragens. Agência Portuguesa do Ambiente. Available online: https://cnpqb.apambiente.pt/gr_barragens/gbportugal/FICHAS/Maratecaficha.htm (accessed on 22 March 2023).
19. DGT. Especificações Técnicas da Carta de Uso E Ocupação do Solo de Portugal Continental Para 1995, 2007, 2010 E 2015; Relatório técnico; Direção-Geral do Território: Lisboa, Portugal, 2018; Available online: http://www.dgterritorio.pt/cartografia_e_geodesia/cartografia/cartografia_tematica/cartografia_de_uso_e_ocupacao_do_solo_cos_clc_e_copernicus/ (accessed on 29 March 2023).
20. DGT. Carta de Uso E Ocupação do Solo. Registo Nacional de Dados Geográficos. SNIG. Direção-Geral do Território: Lisboa, Portugal. Available online: <https://snig.dgterritorio.gov.pt/rndg/srv/por/catalog.search#/search?resultType=details&sortBy=referenceDateOrd&anySnig=COS&fast=index&from=1&to=20> (accessed on 29 March 2023).
21. IPMA. Boletins Climatológicos de Portugal Continental. Instituto Português do Mar E da Atmosfera. Available online: <https://www.ipma.pt/pt/publicacoes/boletins.jsp?cmbDep=cli&cmbTema=pcl&idDep=cli&idTema=pcl&curAno=-1> (accessed on 29 March 2023).
22. Navarro, G.; Caballero, I.; Silva, G.; Parra, P.-C.; Vázquez, Á.; Caldeira, R. Evaluation of forest fire on Madeira Island using Sentinel-2A MSI imagery. *Int. J. Appl. Earth Obs. Geoinf.* **2017**, *58*, 97–106. [CrossRef]
23. Llorens, R.; Sobrino, J.A.; Fernández, C.; Fernández-Alonso, J.M.; Vega, J.A. A methodology to estimate forest fires burned areas and burn severity degrees using Sentinel-2 data. Application to the October 2017 fires in the Iberian Peninsula. *Int. J. Appl. Earth Obs. Geoinf.* **2021**, *95*, 102243. [CrossRef]
24. Gulácsi, A.; Kovács, F. Drought Monitoring with Spectral Indices Calculated From Modis Satellite Images In Hungary. *J. Environ. Geogr.* **2015**, *8*, 11–20. [CrossRef]
25. EOS NDVI FAQ. All You Need To Know About Index. Available online: <https://eos.com/blog/ndvi-faq-all-you-need-to-know-about-ndvi/> (accessed on 13 September 2022).
26. Lamparelli, M. Graus de Trofia em Corpos D'Água do Estado de Sao Paulo: Avaliacao dos Métodos de Monitoramento. Ph.D. Thesis, Universidade de São Paulo, São Paulo, Brazil, 2004. [CrossRef]

27. Ha, N.; Dzung, D.; Hang, H.; Huy, T.; Tu, N. Water quality assessment and eutrophic classification of Hanoi lakes using different indices. *Vietnam J. Agric. Sci.* **2021**, *4*, 1229–1240. [\[CrossRef\]](#)
28. Nojavan, A.F.; Kreakie, B.J.; Hollister, J.W.; Qian, S.S. Rethinking the lake trophic state index. *PeerJ* **2019**, *7*, e7936. [\[CrossRef\]](#) [\[PubMed\]](#)
29. Xu, F.-L.; Jiao, Y. Trophic Classification for Lakes. In *Encyclopedia of Ecology*, 2nd ed.; Elsevier: Oxford, UK, 2019; pp. 487–494. ISBN 978-0-444-64130-4.
30. Dodds, W.K.; Jones, J.R.; Welch, E.B. Suggested classification of stream trophic state: Distributions of temperate stream types by chlorophyll, total nitrogen, and phosphorus. *Water Res.* **1998**, *32*, 1455–1462. [\[CrossRef\]](#)
31. Klippel, G.; Macêdo, R.L.; Branco, C.W.C. Comparison of different trophic state indices applied to tropical reservoirs. *Lakes Reserv. Sci. Policy Manag. Sustain. Use* **2020**, *25*, 214–229. [\[CrossRef\]](#)
32. Carlson, R.E. A trophic state index for lakes1. *Limnol. Oceanogr.* **1977**, *22*, 361–369. [\[CrossRef\]](#)
33. Lillesand, T.; Kiefer, R. *Remote Sensing and Image Interpretation*; John Wiley & Sons: Hoboken, NJ, USA, 1994; 376p.
34. Spyrakos, E.; O'Donnell, R.; Hunter, P.D.; Miller, C.; Scott, M.; Simis, S.G.H.; Neil, C.; Barbosa, C.C.F.; Binding, C.E.; Bradt, S.; et al. Optical types of inland and coastal waters. *Limnol. Oceanogr.* **2018**, *63*, 846–870. [\[CrossRef\]](#)
35. Cohen, J. A coefficient of agreement for nominal scales. *Educ. Psychol. Meas.* **1960**, *20*, 37–46. [\[CrossRef\]](#)
36. DR. Decreto-Lei n°152/2017 de 7 de Dezembro. Diário da República, I Série-no 235/2017 de 7 de Dezembro. Available online: <https://dre.pt/dre/detalhe/decreto-lei/152-2017-114315242> (accessed on 29 March 2023).
37. Liu, J.; Zhang, Y.; Yuan, D.; Song, X. Empirical estimation of total nitrogen and total phosphorus concentration of urban water bodies in china using high resolution IKONOS multispectral imagery. *Water* **2015**, *7*, 6551–6573. [\[CrossRef\]](#)
38. Guildford, S.J.; Hecky, R.E. Total nitrogen, total phosphorus, and nutrient limitation in lakes and oceans: Is there a common relationship? *Limnol. Oceanogr.* **2000**, *45*, 1213–1223. [\[CrossRef\]](#)
39. Yan, R.; Gao, J. Key factors affecting discharge, soil erosion, nitrogen and phosphorus exports from agricultural polder. *Ecol. Modell.* **2021**, *452*, 109586. [\[CrossRef\]](#)
40. Bulgakov, N.G.; Levich, A.P. The nitrogen: Phosphorus ratio as a factor regulating phytoplankton community structure. *Arch. Für Hydrobiol.* **1999**, *146*, 3–22. [\[CrossRef\]](#)

Disclaimer/Publisher's Note: The statements, opinions and data contained in all publications are solely those of the individual author(s) and contributor(s) and not of MDPI and/or the editor(s). MDPI and/or the editor(s) disclaim responsibility for any injury to people or property resulting from any ideas, methods, instructions or products referred to in the content.